Science Advances
AAAS

advances.sciencemag.org/cgi/content/full/6/21/eaaz5156/DC1

Supplementary Materials for

Flexible low-voltage high-frequency organic thin-film transistors

James W. Borchert*, Ute Zschieschang, Florian Letzkus, Michele Giorgio, R. Thomas Weitz, Mario Caironi, Joachim N. Burghartz, Sabine Ludwigs, Hagen Klauk*

*Corresponding author. Email: j.borchert@fkf.mpg.de (J.W.B.); h.klauk@fkf.mpg.de (H.K.)

Published 20 May 2020, *Sci. Adv.* **6**, eaaz5156 (2020)
DOI: 10.1126/sciadv.aaz5156

This PDF file includes:

S1: Contact resistance, carrier mobility and transit frequency

The contact resistance (R_C) in organic TFTs is typically evaluated in the linear regime of transistor operation using the transmission line method (TLM; see Figs. 2 and S4) (*41*). In TLM analyses, as well as for most other methods for determining R_C (*42*), a requirement (and indeed a drawback) is that it is only valid for the linear regime of operation using vanishingly-small V_{DS}, since a key assumption of TLM is that R_C is Ohmic and that the channel resistance is uniform over the entire channel region. This latter point by itself precludes any analysis of R_C in the saturation regime using TLM because of the pinch-off of the channel that occurs when V_{DS} is approximately equivalent to the overdrive voltage (V_{GS}-V_{th}). Experimental investigations have shown that R_C in organic TFTs can vary significantly with V_{DS} (*32*, *43*). Especially for TFTs with small channel lengths (L), R_C may be reduced by V_{DS} due to effects such as image-force lowering (IFL) (*33*) or by drain-induced barrier lowering (DIBL) (*35*) of the injection barrier at the interface between the source contact and the semiconductor. Enhancements of the carrier mobility in the vicinity of the contacts through a Poole-Frenkel-like dependence of the mobility on the applied electric field may also lead to lower R_C, in part due to the nonlinear effects on both charge transport (*44*) and charge injection (*45*). For these reasons it is beneficial to be able to quantify the dependence of R_C on V_{DS}.

Here, we estimate R_C and the intrinsic channel mobility (μ_0) in the saturation regime ($V_{DS} \leq V_{GS} - V_{th}$ for p-channel TFTs) by fitting the transit frequency (f_T) extracted from *S*-parameter measurements as a function of channel length (L). Similar to TLM, we use μ_0 and the width-normalized contact resistance (R_CW) as fitting parameters. This approach has to our knowledge never been explicitly implemented, though comparisons of calculated f_T to experimental results using R_C determined from TLM have been reported (*16*, *36*). In both approaches, the error in the extracted values is assessed simply as the calculated standard error from the fits. In the TLM, the width-normalized total source-to-drain resistance of the TFT (RW) is fit with a linear function with respect to L. In our method, the f_T data as a function of L is fit using the equation derived in the following.

The dependence of the effective mobility (μ_{eff}) and the transit frequency (f_T) on R_C can be illustrated with the following two equations for TFTs operated in the saturation regime (*2*, *46*):

$$\mu_{eff} = \mu_0 \left[1 - \left(\frac{\mu_0 C_{diel} R_C W (V_{GS} - V_{th})}{L + \mu_0 C_{diel} R_C W (V_{GS} - V_{th})}\right)^2\right] \qquad (1)$$

$$f_T = \frac{\mu_{eff}(V_{GS} - V_{th})}{2\pi L \left(L_{ov,total} + \frac{2}{3}L\right)} \qquad (2)$$

where C_{diel} is the gate-dielectric capacitance per unit area and $L_{ov,total}$ is the total gate-to-contact overlap length, which is simply the sum of the gate-to-source ($L_{ov,GS}$) and gate-to-drain ($L_{ov,\,GD}$) overlap lengths. In principle, the term R_C encompasses contributions from both the source and drain contacts. Equation 1 can be simplified to (*36*)

$$\mu_{eff} = \frac{\mu_0}{1 + \frac{1}{2L}\mu_0 C_{diel} R_C W (V_{GS} - V_{th})} \qquad (3)$$

Combining Equations 2 and 3, we then obtain an expression for f_T that includes the influence of the contact resistance:

$$f_T = \frac{\mu_0 (V_{GS} - V_{th})}{2\pi \left(L + \frac{1}{2}\mu_0 C_{diel} R_C W (V_{GS} - V_{th})\right)\left(L_{ov,total} + \frac{2}{3}L\right)} \qquad (4)$$

For illustrative purposes, several curves of the transit frequency as a function of the channel length calculated using Equation 4 and assuming different values for R_CW are shown in Fig. S7.

Supplementary Figures

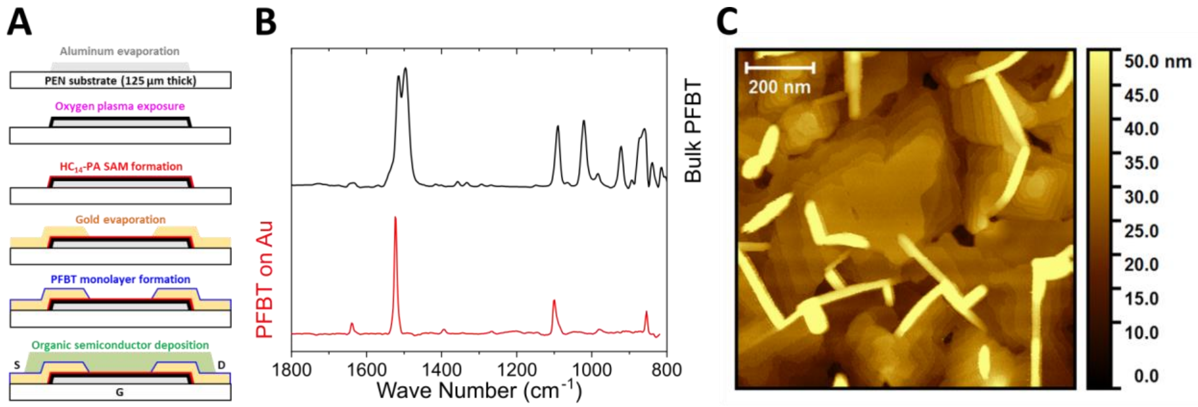

Fig. S1| Device fabrication process and materials characterization. (A) Schematic process flow for the fabrication of bottom-gate bottom-contact (inverted coplanar) organic TFTs. All metal and semiconductor layers are deposited by thermal evaporation or sublimation in vacuum and patterned using high-resolution silicon stencil masks. **(B)** Infrared reflection absorption spectroscopy (IRRAS) analysis of bulk pentafluorobenzenethiol (PFBT, black) and of a chemisorbed monolayer of PFBT on a gold surface (red). **(C)** AFM height scan of a thin film of the organic semiconductor DPh-DNTT deposited onto a hybrid AlO_x/SAM gate dielectric on a flexible PEN substrate.

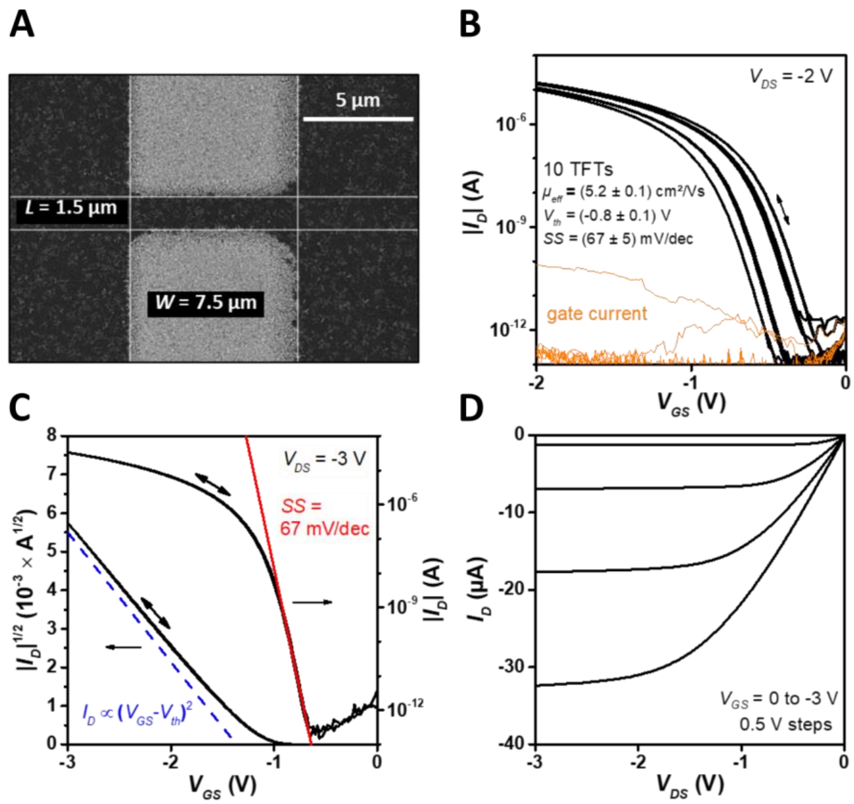

Fig. S2| Static transistor characteristics and uniformity. (A) SEM micrograph of an individual DPh-DNTT TFT. **(B)** Measured transfer characteristics of 10 nominally identical TFTs having a channel length (L) of 1.5 µm, a total gate-to-contact overlap ($L_{ov,total}$) of 60 µm and a channel width (W) of 7.5 µm, with statistics for the effective carrier mobility (μ_{eff}), threshold voltage (V_{th}) and subthreshold swing (SS). **(C)** Transfer characteristics of an individual TFT measured at a drain-source voltage (V_{DS}) of -3 V. The dotted blue line is a guide to the eye, indicating the ideal quadratic dependence of the drain current on the gate-overdrive voltage ($V_{GS} – V_{th}$) in the saturation regime. **(D)** Output characteristics for gate-source voltages (V_{GS}) from 0 to -3 V in steps of 0.5 V.

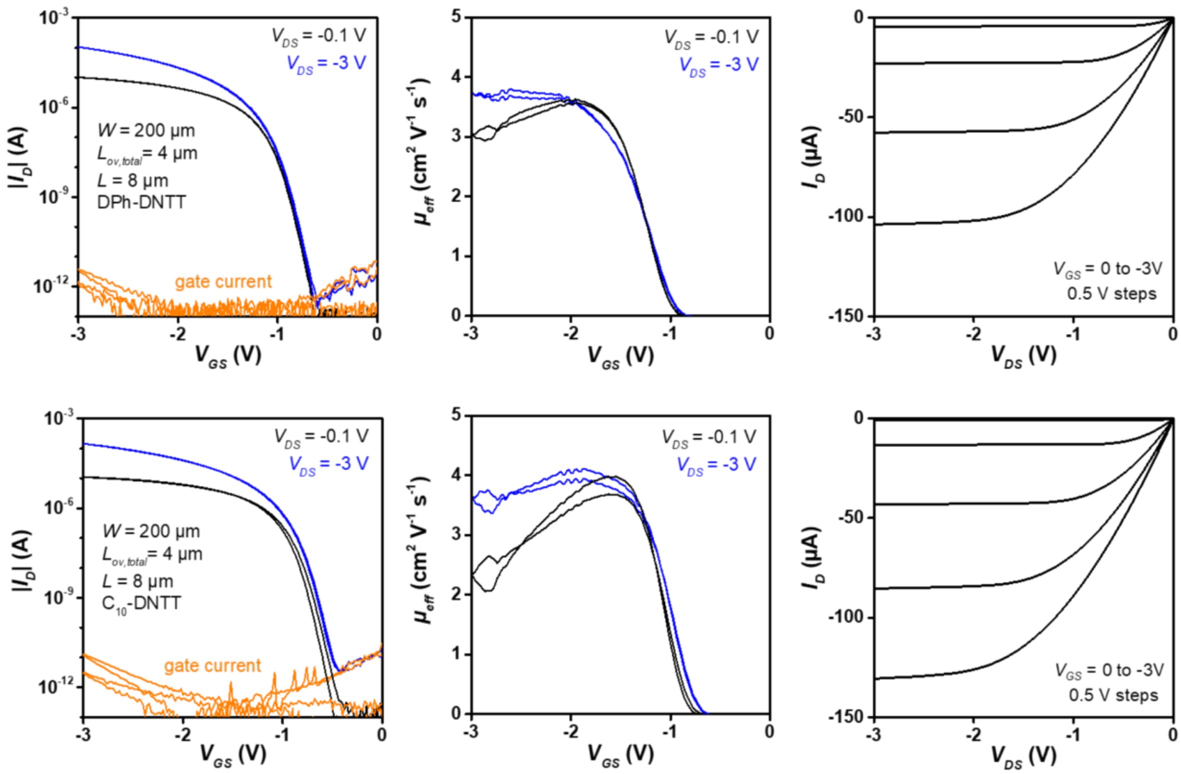

Fig. S3| Static characteristics of TFTs based on DPh-DNTT (top row) and C_{10}-DNTT (bottom row). Both TFTs have a channel length (L) of 8 µm, a total gate-to-contact overlap ($L_{ov,total}$) of 4 µm and a channel width (W) of 200 µm. From left to right: Transfer characteristics, effective carrier mobility (μ_{eff}) plotted as a function of the gate-source voltage, and output characteristics for gate-source voltages (V_{GS}) from 0 to -3 V in steps of 0.5 V. (Note that these TFTs were fabricated separately from the TFTs shown in Fig. S2.)

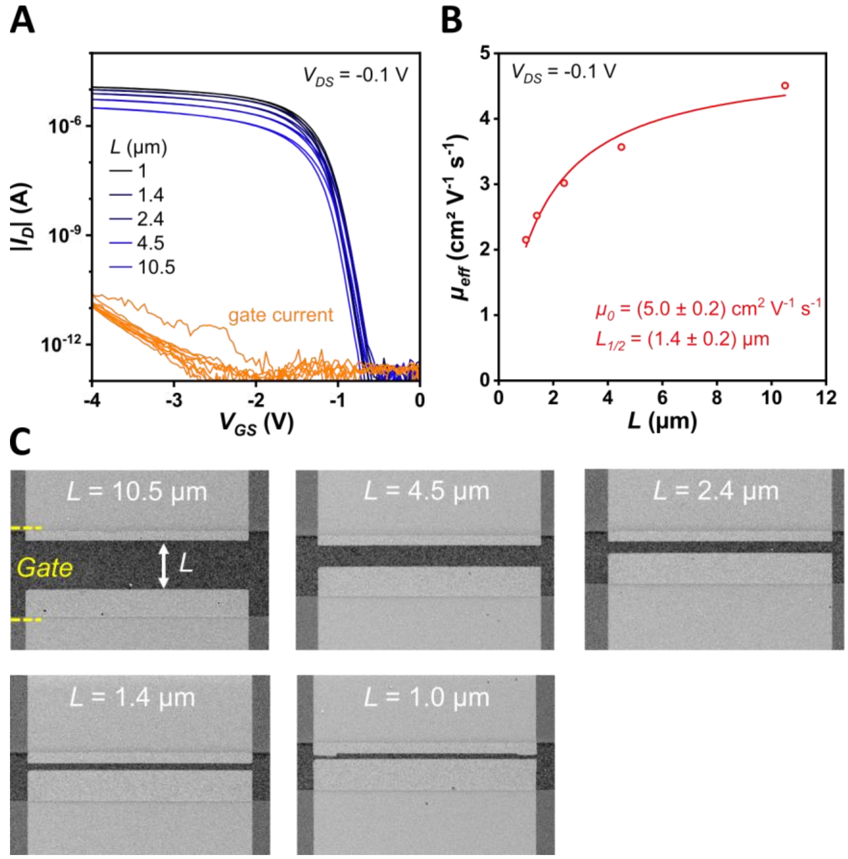

Fig. S4| Transistors for TLM analysis. (A) Transfer characteristics of DPh-DNTT TFTs with channel lengths (L) ranging from 1 to 10.5 µm and a channel width (W) of 50 µm, measured with a drain-source voltage (V_{DS}) of -0.1 V. **(B)** Effective carrier mobility (μ_{eff}) in the linear regime determined for each TFT as a function of the channel length (L). The line is a fit to the data using the equation $\mu_{eff} = \mu_0 \, (1 + L_{1/2}/L)^{-1}$ where μ_0 is the intrinsic channel mobility and $L_{1/2}$ is the channel length at which $\mu_{eff} = ½ \, \mu_0$. **(C)** SEM micrographs of the channel region of the TFTs. (Note that these TFTs were fabricated separately from the TFTs shown in Fig. S2.)

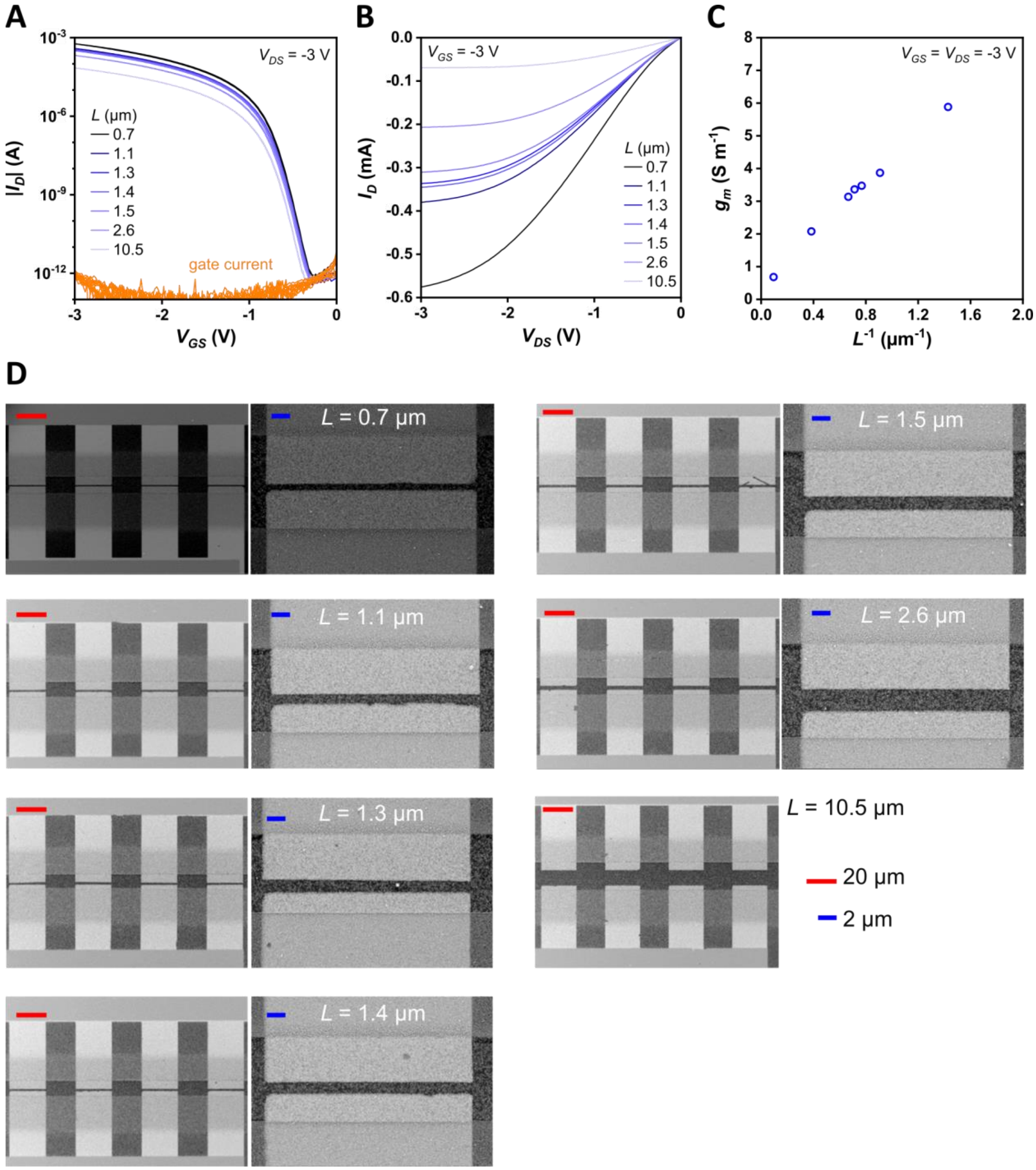
A
V_{DS} = -3 V
$|I_D|$ (A)
V_{GS} (V)
L (μm)
0.7
1.1
1.3
1.4
1.5
2.6
10.5
gate current
B
V_{GS} = -3 V
I_D (mA)
V_{DS} (V)
C
V_{GS} = V_{DS} = -3 V
g_m (S m^{-1})
L^{-1} (μm^{-1})
D
L = 0.7 μm
L = 1.1 μm
L = 1.3 μm
L = 1.4 μm
L = 1.5 μm
L = 2.6 μm
L = 10.5 μm
20 μm
2 μm

Fig. S5| Transistors for *S*-parameter measurements. (A) Transfer characteristics of DPh-DNTT TFTs with channel lengths (L) ranging from 0.7 to 10.5 µm, a total gate-to-contact overlap ($L_{ov,total}$) of 10 µm and a channel width (W) of 100 µm, measured with a drain-source voltage (V_{DS}) of -3 V. **(B)** Output characteristics of each TFT for a gate-source voltage (V_{GS}) of -3 V. **(C)** Channel-width-normalized peak transconductance (g_m) at a gate-source voltage (V_{GS}) of -3 V as a function of the inverse of the channel length. **(D)** SEM micrographs of the channel region of the TFTs. (Note that these TFTs were fabricated separately from the TFTs shown in Fig. S2.)

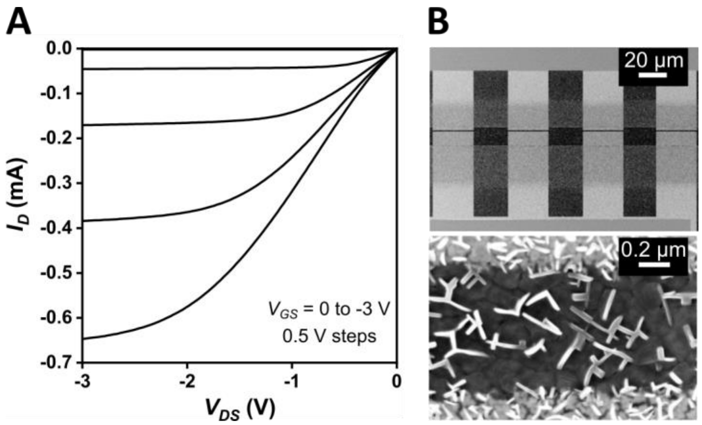

Fig. S6| DPh-DNTT TFT showing a transit frequency of 21 MHz. The TFT has a channel length (*L*) of 0.6 µm, a total gate-to-contact overlap ($L_{ov,total}$) of 10 µm and a channel width (*W*) of 100 µm. **(A)** Output characteristics for gate-source voltages (V_{GS}) from 0 to -3 V in steps of 0.5 V. **(B)** SEM micrographs of the channel region of the TFT.

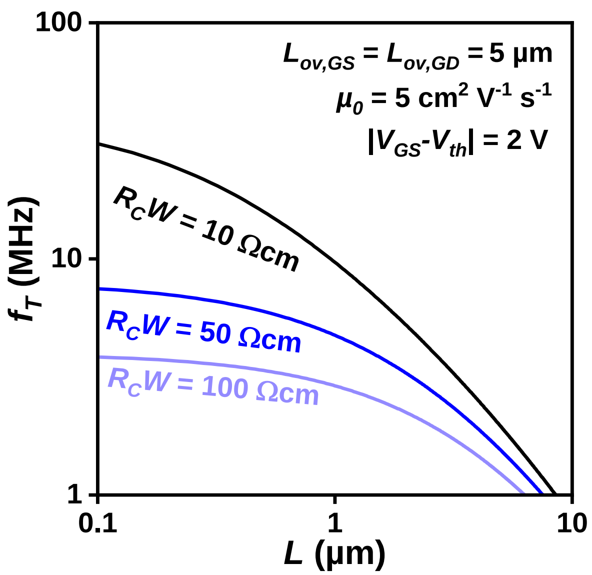

Fig. S7| Relation between channel length, contact resistance and transit frequency. The curves were calculated using Equation (4) for width-normalized contact resistances (R_CW) of 10, 50 and 100 Ωcm, gate-to-source and gate-to-drain overlaps ($L_{ov,GS}$, $L_{ov,GD}$) of 5 µm, an intrinsic channel mobility (μ_0) of 5 cm^2/Vs and a gate-overdrive voltage ($|V_{GS}-V_{DS}|$) of 2 V.

Table S1| Literature review of voltage-normalized transit frequencies reported for organic TFTs.

Reference	Substrate	Device	Voltage (V)	f_T/V (MHz V^{-1})
Brown, Science, vol. 270, p. 972, 1995	Rigid	RO*	20	$1.25 \cdot 10^{-4}$
Crone, J. Appl. Phys., vol. 89, p. 5125, 2001	Rigid	RO*	100	$5 \cdot 10^{-4}$
Baude, Appl. Phys. Lett., vol. 82, p. 3964, 2003	Rigid	RO*	50	$6.67 \cdot 10^{-4}$
Sheraw, Int'l Electr. Dev. Meeting 2000	Flexible	RO*	20	0.00125
Fix, Appl. Phys. Lett., vol. 81, p. 1735, 2002	Flexible	RO*	80	0.0092
Wagner, Appl. Phys. Lett., vol. 89, p. 243515, 2006	Rigid	RO*	10	0.2
Heremans, Int'l Electr. Dev. Meeting 2009	Flexible	RO*	20	0.2
Zschieschang, Org. Electronics, vol. 14, p. 1516, 2013	Flexible	RO*	4	0.42
Kitamura, Appl. Phys. Lett., vol. 95, p. 023503, 2009	Rigid	TFT[a]	25	0.8
Kitamura, Jpn. J. Appl. Phys., vol. 50, p. 01BC01, 2011	Rigid	TFT[a]	25	1.11
Zaki, Org. Electronics, vol. 14, p. 1318, 2013	Rigid	TFT[b]	3	1.37
Nakayama, Adv. Mater. Interfaces, vol. 1, p. 1300124, 2014	Rigid	TFT[a]	10	1.9
Yamamura, Sci. Adv., vol. 4, p. eaao5758, 2018	Rigid	TFT[a]	10	2
Perinot, Adv. Sci., vol. 6, p. 1801566, 2019	Flexible	TFT[a]	14	2.06
Borchert, Int'l Electr. Dev. Meeting 2018	Flexible	TFT[b]	3	2.23
Kheradmand-Boroujeni, Sci. Rep., vol. 8, p. 7643, 2018	Rigid	TFT[c]	8.6	4.65
This work	Flexible	TFT[b]	3	7

[a] Small-signal currents directly measured to evaluate f_T.

[b] S-parameter measurement to evaluate f_T.

[c] Pulsed-bias measurement circuit to evaluate f_T.

*In cases where the data were obtained from measurements on ring oscillators (RO), the equivalent frequency $f_{eq} = 1/(2\tau)$ is normalized to the supply voltage.

REFERENCES

1. X. Guo, Y. Xu, S. Ogier, T. N. Ng, M. Caironi, A. Perinot, L. Li, J. Zhao, W. Tang, R. A. Sporea, A. Nejim, J. Carrabina, P. Cain, F. Yan, Current status and opportunities of organic thin-film transistor technologies. *IEEE Trans. Electron Devices* **64**, 1906–1921 (2017).

2. A. Perinot, M. Giorgio, M. Caironi, Development of organic field-effect transistors for operation at high frequency, in *Flexible Carbon-Based Electronics*, V. Palermo, P. Samorì, Eds. (Wiley-VCH, ed. 1, 2018), 71–94.

3. K. Myny, The development of flexible integrated circuits based on thin-film transistors. *Nat. Electron.* **1**, 30–39 (2018).

4. D. Hsieh, *Flat Panel Display Market & Technology Outlook*, (2017); https://technology.ihs.com/594467/flat-panel-display-market-outlook-2017

5. Y. Kubota, T. Matsumoto, H. Tsuji, N. Suzuki, S. Imai, H. Kobayashi, T. Matsumoto, H. Tsuji, N. Suzuki, S. Imai, H. Kobayashi, 1.5-V-operation ultralow power circuit of poly-si TFTs fabricated using the NAOS method. *IEEE Trans. Electron Devices* **59**, 385–392 (2012).

6. X. Yu, T. J. Marks, A. Facchetti, Metal oxides for optoelectronic applications. *Nat. Mater.* **15**, 383–396 (2016).

7. H. Klauk, Will we see gigahertz organic transistors? *Adv. Electron. Mater.* **4**, 1700474 (2018).

8. D. J. Gundlach, L. Zhou, J. A. Nichols, T. N. Jackson, P. V. Necliudov, M. S. Shur, An experimental study of contact effects in organic thin film transistors. *J. Appl. Phys.* **100**, 024509 (2006).

9. P. V. Pesavento, K. P. Puntambekar, C. D. Frisbie, J. C. McKeen, P. P. Ruden, Film and contact resistance in pentacene thin-film transistors: Dependence on film thickness, electrode geometry, and correlation with hole mobility. *J. Appl. Phys.* **99**, 094504 (2006).

10. M. Gruber, E. Zojer, F. Schürrer, K. Zojer, Impact of materials versus geometric parameters on the contact resistance in organic thin-film transistors. *Adv. Funct. Mater.* **23**, 2941–2952 (2013).

11. K. Zojer, E. Zojer, A. F. Fernandez, M. Gruber, Impact of the capacitance of the dielectric on the contact resistance of organic thin-film transistors. *Phys. Rev. Appl.* **4**, 044002 (2015).

12. J. W. Borchert, B. Peng, F. Letzkus, J. N. Burghartz, P. K. L. Chan, K. Zojer, S. Ludwigs, H. Klauk, Small contact resistance and high-frequency operation of flexible low-voltage inverted coplanar organic transistors. *Nat. Commun.* **10**, 1119 (2019).

13. B. Stadlober, U. Haas, H. Gold, A. Haase, G. Jakopic, G. Leising, N. Koch, S. Rentenberger, E. Zojer, Orders-of-magnitude reduction of the contact resistance in short-channel hot embossed organic thin film transistors by oxidative treatment of Au-electrodes. *Adv. Funct. Mater.* **17**, 2687–2692 (2007).

14. A. Kahn, N. Koch, W. Gao, Electronic structure and electrical properties of interfaces between metals and π-conjugated molecular films. *J. Polym. Sci. Part B Polym. Phys.* **41**, 2529–2548 (2003).

15 D. Braga, M. Ha, W. Xie, C. D. Frisbie, Ultralow contact resistance in electrolyte-gated organic thin film transistors. *Appl. Phys. Lett.* **97**, 193311 (2010).

16. A. Yamamura, S. Watanabe, M. Uno, M. Mitani, C. Mitsui, J. Tsurumi, N. Isahaya, Y. Kanaoka, T. Okamoto, J. Takeya, Wafer-scale, layer-controlled organic single crystals for high-speed circuit operation. *Sci. Adv.* **4**, eaao5758 (2018).

17. N. Münzenrieder, G. A. Salvatore, L. Petti, C. Zysset, L. Büthe, C. Vogt, G. Cantarella, G. Tröster, Contact resistance and overlapping capacitance in flexible sub-micron long oxide thin-film transistors for above 100 MHz operation. *Appl. Phys. Lett.* **105**, 263504 (2014).

18. Z. Zhang, S. O. Koswatta, S. W. Bedell, A. Baraskar, M. Guillorn, S. U. Engelmann, Y. Zhu, J. Gonsalves, A. Pyzyna, M. Hopstaken, C. Witt, L. Yang, F. Liu, J. Newbury, W. Song, C. Cabral, M. Lofaro, A. S. Ozcan, M. Raymond, C. Lavoie, J. W. Sleight, K. P. Rodbell, P. M. Solomon, Ultra low contact resistivities for CMOS beyond 10-nm node. *IEEE Electron Device Lett.* **34**, 723–725 (2013).

19. F. Letzkus, J. Butschke, B. Höfflinger, M. Irmscher, C. Reuter, R. Springer, A. Ehrmann, J. Mathuni, Dry etch improvements in the SOI wafer flow process for IPL stencil mask fabrication. *Microelectron. Eng.* **53**, 609–612 (2000).

20.T. Zaki, F. Ante, U. Zschieschang, J. Butschke, F. Letzkus, H. Richter, H. Klauk, J. N. Burghartz, A 3.3 V 6-Bit 100 kS/s current-steering digital-to-analog converter using organic p-type thin-film transistors on glass. *IEEE J. Solid State Circuits* **47**, 292–300 (2012).

21. U. Zschieschang, R. Hofmockel, R. Rödel, U. Kraft, M. J. Kang, K. Takimiya, T. Zaki, F. Letzkus, J. Butschke, H. Richter, J. N. Burghartz, H. Klauk, Megahertz operation of flexible low-voltage organic thin-film transistors. *Org. Electron.* **14**, 1516–1520 (2013).

22. K. Niimi, M. J. Kang, E. Miyazaki, I. Osaka, K. Takimiya, General synthesis of dinaphtho[2,3-b:2′,3′-f]thieno[3,2-b]thiophene (DNTT) derivatives. *Org. Lett.* **13**, 3430–3433 (2011).

23. D. Gebeyehu, K. Walzer, G. He, M. Pfeiffer, K. Leo, J. Brandt, A. Gerhard, P. Stößel, H. Vestweber, Highly efficient deep-blue organic light-emitting diodes with doped transport layers. *Synth. Met.* **148**, 205–211 (2005).

24. J. Birnstock, T. Canzler, M. Hofmann, A. Lux, S. Murano, P. Wellmann, A. Werner, PIN OLEDs—Improved structures and materials to enhance device lifetime. *J. Soc. Inf. Disp.* **16**, 221–229 (2008).

25. R. Meerheim, K. Walzer, G. He, M. Pfeiffer, K. Leo, Highly efficient organic light emitting diodes (OLED) for diplays and lighting. *Org. Optoelectron. Photonics II* **6192**, 61920P (2006).

26. M. Elsobky, M. Elattar, G. Alavi, F. Letzkus, H. Richter, U. Zschieschang, M. Strecker, H. Klauk, J. N. Burghartz, A digital library for a flexible low-voltage organic thin-film transistor technology. *Org. Electron.* **50**, 491–498 (2017).

27. S. D. Ogier, H. Matsui, L. Feng, M. Simms, M. Mashayekhi, J. Carrabina, L. Terés, S. Tokito, Uniform, high performance, solution processed organic thin-film transistors integrated in 1 MHz frequency ring oscillators. *Org. Electron.* **54**, 40–47 (2018).

28. T. Zaki, R. Rodel, F. Letzkus, H. Richter, U. Zschieschang, H. Klauk, J. N. Burghartz, S-parameter characterization of submicrometer low-voltage organic thin-film transistors. *IEEE Electron Device Lett.* **34**, 520–522 (2013).

29. M. Giorgio, M. Caironi, Radio-frequency polymer field-effect transistors characterized by S-parameters. *IEEE Electron Device Lett.* **40**, 953–956 (2019).

30. D. A. Frickey, Conversions between S, Z, Y, h, ABCD, and T parameters which are valid for complex source and load impedances. *IEEE Trans. Microw. Theory Tech.* **42**, 205–211 (1994).

31. T. Zaki, S. Scheinert, I. Horselmann, R. Rodel, F. Letzkus, H. Richter, U. Zschieschang, H. Klauk, J. N. Burghartz, Accurate capacitance modeling and characterization of organic thin-film transistors. *IEEE Trans. Electron Devices* **61**, 98–104 (2014).

32. M. Caironi, C. Newman, J. R. Moore, D. Natali, H. Yan, A. Facchetti, H. Sirringhaus, Efficient charge injection from a high work function metal in high mobility *n*-type polymer field-effect transistors. *Appl. Phys. Lett.* **96**, 183303 (2010).

33. D. Natali, M. Caironi, Charge injection in solution-processed organic field-effect transistors: Physics, models and characterization methods. *Adv. Mater.* **24**, 1357–1387 (2012).

34. J. C. Scott, Metal–organic interface and charge injection in organic electronic devices. *J. Vac. Sci. Technol. A.* **21**, 521–531 (2003).

35. S. M. Sze, K. N. Kwok, *Physics of Semiconductor Devices* (John Wiley Sons, Inc, ed. 3, 2007).

36. T. Zaki, R. Rödel, F. Letzkus, H. Richter, U. Zschieschang, H. Klauk, J. N. Burghartz, AC characterization of organic thin-film transistors with asymmetric gate-to-source and gate-to-drain overlaps. *Org. Electron.* **14**, 1318–1322 (2013).

37. A. Perinot, M. Caironi, Accessing MHz operation at 2 V with field-effect transistors based on printed polymers on plastic. *Adv. Sci.* **6**, 1801566 (2019).

38. B. Kheradmand-Boroujeni, M. P. Klinger, A. Fischer, H. Kleemann, K. Leo, F. Ellinger, A Pulse-Biasing Small-Signal Measurement Technique Enabling 40 MHz Operation of Vertical Organic Transistors. *Sci. Rep.* **8**, 7643 (2018).

39. U. Kraft, M. Sejfić, M. J. Kang, K. Takimiya, T. Zaki, F. Letzkus, J. N. Burghartz, E. Weber, H. Klauk, Flexible low-voltage organic complementary circuits: Finding the optimum combination of semiconductors and monolayer gate dielectrics. *Adv. Mater.* **27**, 207–214 (2015).

40. W. Azzam, A. Bashir, P. Ulrich Biedermann, M. Rohwerder, Formation of highly ordered and orientated gold islands: Effect of immersion time on the molecular adlayer structure of pentafluorobenzenethiols (PFBT) SAMs on Au(111). *Langmuir* **28**, 10192–10208 (2012).

41. S. Luan, G. W. Neudeck, An experimental study of the source/drain parasitic resistance effects in amorphous silicon thin film transistors. *J. Appl. Phys.* **72**, 766–772 (1992).

42. C. Liu, Y. Xu, Y.-Y. Noh, Contact engineering in organic field-effect transistors. *Mater. Today* **18**, 79–96 (2015).

43. F. Ante, D. Kälblein, T. Zaki, U. Zschieschang, K. Takimiya, M. Ikeda, T. Sekitani, T. Someya, J. N. Burghartz, K. Kern, H. Klauk, Contact resistance and megahertz operation of aggressively scaled organic transistors. *Small* **8**, 73–79 (2012).

44. L. Li, S. Van Winckel, J. Genoe, P. Heremans, Electric field-dependent charge transport in organic semiconductors. *Appl. Phys. Lett.* **95**, 153301 (2009).

45. J. Li, W. Ou-Yang, M. Weis, Electric-field enhanced thermionic emission model for carrier injection mechanism of organic field-effect transistors: Understanding of contact resistance. *J. Phys. D Appl. Phys.* **50**, 035101 (2017).

46. A. Benor, D. Knipp, Contact effects in organic thin film transistors with printed electrodes. *Org. Electron.* **9**, 209–219 (2008).